

Periodic and quasiperiodic regimes in self-coupled lasers

Li Ruo-Ding* and Paul Mandel

Université Libre de Bruxelles, Campus Plaine Code Postal 231, 1050 Bruxelles, Belgium

T. Erneux

Department of Engineering Sciences and Applied Mathematics, Northwestern University, Evanston, Illinois 60208

(Received 10 November 1989; revised manuscript received 22 December 1989)

We explore the bifurcation diagrams of self-coupled unidirectional single-mode ring lasers. We focus our attention on nearly identical lasers with an intermediate coupling and in the limit where the atomic polarizations can be adiabatically eliminated. We determine analytically the domains of a stable steady state, bounded by Hopf bifurcations. We study the stability of the emerging branch of periodic solutions and in one case determine the presence of a secondary Hopf bifurcation leading to quasiperiodic solutions. These results are complemented by a set of numerically determined bifurcation diagrams that display the behavior of the solutions far from the bifurcation points.

I. INTRODUCTION

In a recent paper¹ (hereafter referred to as I), we have begun a study of a simple model of self-coupled lasers (SCL). Each laser is described as a single-mode unidirectional homogeneously broadened ring laser. The output of each laser is sent, after a suitable intensity attenuation, as an injected signal into the other laser. Hence each laser is the feedback loop for the other laser. For perfect tuning and identical lasers, this problem was considered by Lawandy and co-workers^{2,3} as a model for two coupled Lorenz equations. Since perfectly identical lasers are not experimentally realizable, it is worth considering nearly identical lasers, taking the difference between the two devices as a small parameter. In I, we have shown that such a formulation of the SCL is indeed possible. Another piece of critical behavior that is worth putting on stage is the property displayed by a class of lasers (such as CO₂ and some solid-state lasers) to behave like conservative systems with a weak dissipative perturbation.^{4,5} The conservative system is an oscillator which has an infinite set of bounded periodic orbits. Thus the SCL correspond to a pair of nonlinear oscillators with weak dissipative coupling and perturbation.

A similar set of equations has been studied, though in a different domain of parameters, by Wang and Winful to describe phase-locked semiconductor laser arrays.⁶ In that study the emphasis is on coupling N (typically of the order of 10) semiconductor lasers so that all results are purely numerical. Another study of a similar problem is that of Falvey and Chow⁷ who study the influence of the lasers coupling on the spectrum and mutual coherence due to spontaneous emission. This analytic study is valid for arbitrary lasers coupling and shows a rather sensitive dependence of the results on the inter-laser detuning.

One property of the SCL is the presence of a domain of bistability for the field amplitude versus the control parameters. However, there is at most one stable finite intensity solution. It emerges from an unstable solution at

a limit point. Furthermore, this branch is either stable everywhere or at most one Hopf bifurcation can appear on that stable branch whereas up to three Hopf bifurcations can appear on the stable branch. In this paper we shall focus our attention to the case where either one or two Hopf bifurcations are located near the limit point from which the stable steady state emerges (codimension-2 and codimension-3 bifurcation problems, respectively).

In the domain of parameter space where the only Hopf bifurcation occurs on the stable branch near the limit point, the corresponding canonical problem in bifurcation theory is the interaction of a simple zero root with a pair of imaginary roots (references to the relevant mathematical literature are given in I). In the theory of the laser with an injected signal, an example of such a situation has been considered by Oppo *et al.*⁸ though they studied the problem numerically. Here, on the contrary, we construct the periodic solutions analytically in the vicinity of the Hopf bifurcation and are able to determine their stability property.

Another possibility which we investigate is that two Hopf bifurcations occur near the limit point, one on each side of the limit point or both on the same branch. Here the canonical codimension-3 problem in bifurcation theory has been considered in part by Koncay and Pei Yu.⁹

Most of the results which we will present in this paper are based on analytical studies of the problems. Therefore the near degeneracy of the critical points which occurs when the Hopf bifurcations are near the limit point imply a strong limitation on the domain of validity of the results. To obviate this defect we have complemented our study by a set of numerically determined bifurcation diagrams which enable us to see how the stability evolves at arbitrary distances from criticality.

As shown in I, when the atomic polarization of both lasers can be adiabatically eliminated, the resulting rate equations are

$$\Delta\mu' = (\nu_1 - \nu_2)/\kappa_1 - [\beta_1\alpha(E_2/E_1) + k\beta_2(E_1/\alpha E_2)]\sin(\Delta\mu), \quad (1.1a)$$

$$E_1' = E_1(A_1F_1 - 1) + \beta_1\alpha E_2\cos(\Delta\mu), \quad (1.1b)$$

$$F_1' = -\gamma_1[-1 + (E_1^2 + 1)F_1], \quad (1.1c)$$

$$E_2' = kE_2(A_2F_2 - 1) + k\beta_2(E_1/\alpha)\cos(\Delta\mu), \quad (1.1d)$$

$$F_2' = -\gamma_2[-1 + (E_2^2 + 1)F_2]. \quad (1.1e)$$

The indices 1 and 2 refer to the two lasers. E_j are the field amplitudes with decay rates κ_j , and F_j are the population inversions (normalized to 1) with decay rates γ_j . Each laser is also characterized by a frequency ν_j and a pump parameter A_j . The time is scaled to the decay rate κ_1 of the electric field E_1 so that $k = \kappa_2/\kappa_1$. Finally, the parameter α is the ratio of the saturation amplitudes and β_j is associated with the amplitude attenuation suffered by the field injected in the cavity j .

As in I we shall consider that the two lasers are identical in amplifying material and design. Hence we take

$$\alpha = 1, \quad k = 1, \quad \gamma_1 = \gamma_2 = \gamma. \quad (1.2)$$

The smallness parameter is chosen as the common decay rate γ so that

$$\gamma \ll 1. \quad (1.3)$$

This parameter is of the order of 10^{-4} for low-pressure CO_2 lasers and for $\text{Nd}^{3+}:\text{YAG}$ (where YAG stands for yttrium aluminum garnet) lasers when operating in the single-mode regime.¹⁰ Furthermore, for these lasers experimental results indicate that rate equations with the assumption of homogeneous broadening is valid. In this paper we shall continue our investigation of the moderate coupling between the SCL. More explicitly, we shall consider the following domain of parameters:

$$\Theta = (\nu_1 - \nu_2)/\kappa_1 = O(\gamma^{1/2}), \quad (1.4a)$$

$$\beta_1, \beta_2 = O(\gamma^{1/2}), \quad (1.4b)$$

$$A_1 - 1, A_2 - 1 = O(1), \quad > 0. \quad (1.4c)$$

This leads to a frequency mismatch $\nu_1 - \nu_2$ of the order of 0.1–1 MHz and a transmission of 1% of the output field of each laser into the other laser. Conditions (1.4a) and (1.4b) define the moderate coupling domain. In I we considered the alternative constraint

$$A_1 - 1 = A_2 - 1 = O(\gamma^{1/2}), \quad (1.5)$$

which restricted the study to the vicinity of the laser first threshold. This restriction will be removed in this paper in order to avoid effects related to the critical slowing down due to the proximity of the lasing first threshold.

In the parameter domain (1.4) the system of equations Eqs. (1.1) has steady solutions with a domain of coexistence as shown on Figs. 1(a) and 1(b). These solutions correspond to a phase-locked regime since $\Delta\mu$ is constant. They can be classified according to their behavior in the limit β_1 and $\beta_2 \rightarrow 0$:

$$\text{solution (1)} \quad E_1 \rightarrow (A_1 - 1)^{1/2}, \quad E_2 \rightarrow (A_2 - 1)^{1/2};$$

$$\text{solution (2)} \quad E_1 \rightarrow (A_1 - 1)^{1/2}, \quad E_2 \rightarrow (A_2 - 1)^{1/2};$$

$$\text{solution (3)} \quad E_1 \rightarrow 0, \quad E_2 \rightarrow (A_2 - 1)^{1/2};$$

$$\text{solution (4)} \quad E_1 \rightarrow (A_1 - 1)^{1/2}, \quad E_2 \rightarrow 0.$$

Solutions (2)–(4) are unstable for β_1 and β_2 strictly different from 0. Solution (1), however, may have a finite domain of stability. In this paper we shall study the stability of this solution in the vicinity of the limit point which is common to both E_1 and E_2 . Since we shall use the intercavity detuning as parameter, we have displayed on Figs. 1(c) and 1(d) the two field amplitudes versus θ , which is proportional to $\nu_1 - \nu_2$ [see the definitions (1.6)]. The solutions are labeled with the same number as their corresponding four curves in Fig. 1. When (1.5) holds instead of (1.4c), no Hopf bifurcation to periodic solutions was possible and the steady-state solution (1) on the upper branch of the hysteresis was stable. On the contrary, when the full set of parameters (1.4) is used, Hopf bifurcation points can appear on the stable and unstable finite intensity branches of solutions. The purpose of this paper is to study the particular case when these Hopf bifurcations are near to the limit point and therefore interact with it

We introduce the notation

$$\gamma^{1/2} = \epsilon$$

and define the following scaled variables:

$$\beta_j = \epsilon b_j, \quad A_j F_j - 1 = \epsilon W_j, \quad (\nu_1 - \nu_2)/\kappa_1 = \epsilon \theta, \quad (1.6)$$

$$\tau = \epsilon t, \quad A_j - 1 = a_j^2.$$

Let $E_j = a_j = O(1)$ be the steady field amplitudes at the limit point. In order for a steady-state solution to exist, it is necessary from Eq. (1.1a) that the following condition be verified:

$$\theta = (\nu_1 - \nu_2)/(\epsilon\kappa_1) < \theta_L \equiv (b_1 a_2^2 + b_2 a_1^2)/(a_1 a_2). \quad (1.7)$$

We take θ as our control parameter because the difference of cavity frequencies can easily be controlled experimentally. Thus we set

$$\theta = \theta_L + \epsilon^2 D \quad (1.8)$$

and introduce two time scales

$$T = \tau, \quad s = \epsilon\tau \quad (1.9)$$

in terms of which the dependent variables are expressed as

$$\Delta\mu(T, s) = \pi/2 + \epsilon\psi_1 + \epsilon^2\psi_2 + \dots,$$

$$E_1(T, s) = a_1 + \epsilon X_1 + \epsilon^2 X_2 + \dots,$$

$$E_2(T, s) = a_2 + \epsilon \bar{X}_1 + \epsilon^2 \bar{X}_2 + \dots,$$

$$W_1(T, s) = \epsilon Y_1 + \epsilon^2 Y_2 + \dots,$$

$$W_2(T, s) = \epsilon \bar{Y}_1 + \epsilon^2 \bar{Y}_2 + \dots.$$

To first order in ϵ we obtain the following set of coupled equations:

$$\frac{d\psi_1}{dT} \equiv \psi_{1T} = [(b_1 a_2^2 - b_2 a_1^2) / (a_1^2 a_2^2)] \times (a_2 X_1 + a_1 \bar{X}_1), \tag{1.10a}$$

$$X_{1T} = a_1 Y_1 - b_1 a_2 \psi_1, \tag{1.10b}$$

$$Y_{1T} = -2a_1 X_1, \tag{1.10c}$$

$$\bar{X}_{1T} = a_2 \bar{Y}_1 - b_2 a_1 \psi_1, \tag{1.10d}$$

$$\bar{Y}_{1T} = -2a_2 \bar{X}_1. \tag{1.10e}$$

In Sec. II we shall study the case where the two self-

coupled laser differ only by the amount of intensity attenuation before reinjection, whereas in Sec. III we concentrate on the case where the two lasers differ only by the optical pump parameters. In this last section we first present an analytic study followed by a numerical investigation of the bifurcation diagrams far from the limit points.

II. IDENTICAL PUMP PARAMETERS BUT DIFFERENT COUPLING

In this section we analyze Eqs. (1.10) when the pump parameters are identical but the coupling constants are different:

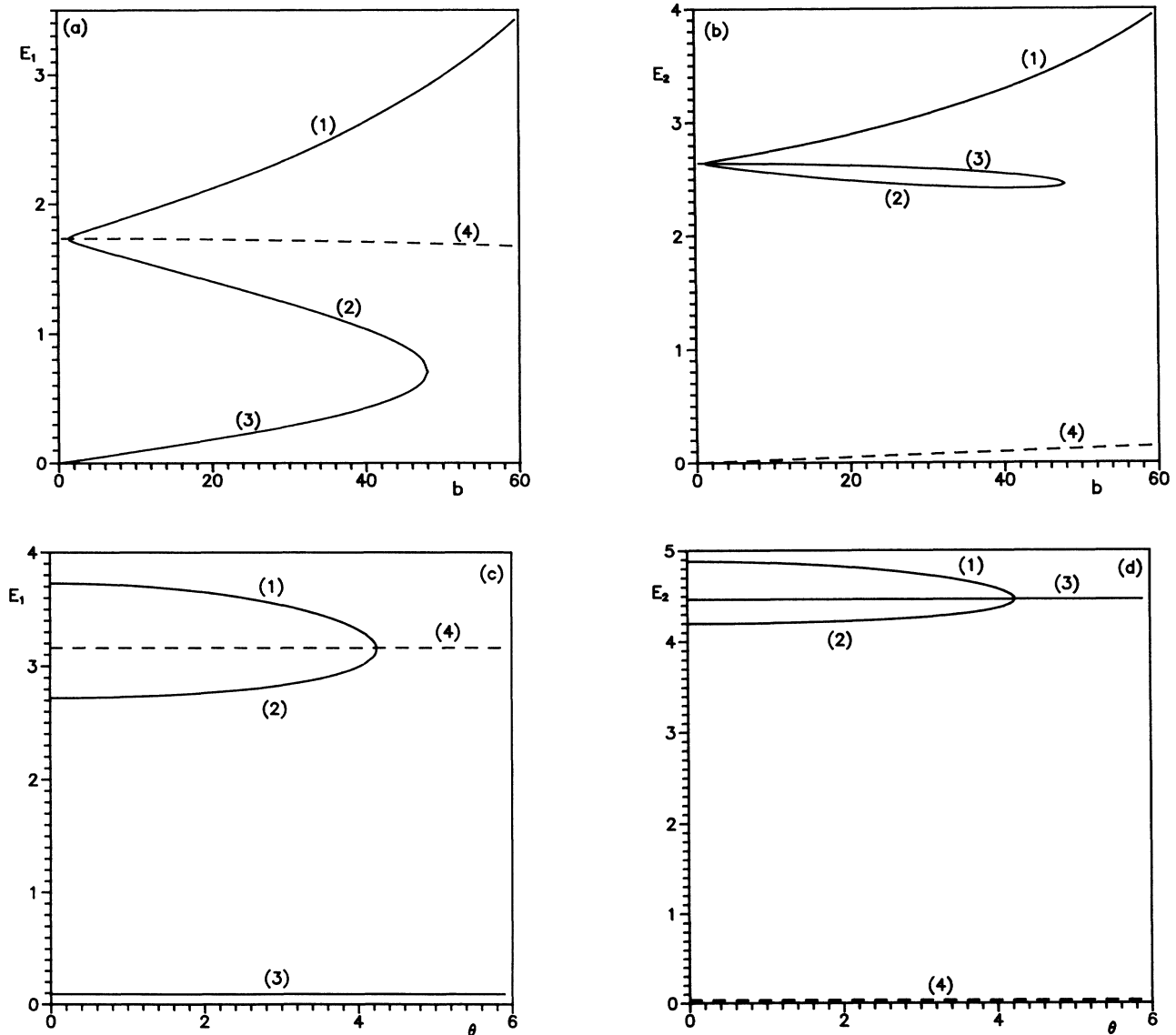


FIG. 1. The four possible steady-state solutions of Eqs. (1.1) are displayed for the field amplitudes E_j vs the parameter b in (a) and (b), vs θ in (c) and (d). The other parameters are $A_1=3$, $A_2=7$, and $\theta=3$ for (a) and (b), whereas $A_1=11$, $A_2=21$, $B=2$, and $\epsilon=0.1$ for (c) and (d).

$$a_1 = a_2 = a, \quad b_1 \neq b_2. \quad (2.1)$$

For definiteness, we take $\Delta b = b_2 - b_1 > 0$. It is then straightforward to solve Eqs. (1.10) to obtain

$$\begin{aligned} \mathbf{Z}(T, s) = & \eta(s)\mathbf{Z}_1 + \zeta(s)\mathbf{Z}_2 \exp(\lambda_2 T) \\ & + \xi(s)\mathbf{Z}_3 \exp(\lambda_3 T) + \text{c.c.} \end{aligned} \quad (2.2)$$

where

$$\begin{aligned} \mathbf{Z} = & \text{col}(\psi_1, X_1, Y_1, \bar{X}_1, \bar{Y}_1), \\ \mathbf{Z}_1 = & \text{col}(1, 0, b_1, 0, b_1 + \Delta b), \end{aligned} \quad (2.3)$$

$$\begin{aligned} \mathbf{Z}_2 = & \text{col}\{(\Delta b)^2, ib_1 a [2a^2 + (\Delta b)^2]^{1/2}, \\ & -2b_1 a^2, i(b_1 + \Delta b)a [2a^2 + (\Delta b)^2]^{1/2}, \\ & -2(b_1 + \Delta b)a^2\}, \end{aligned} \quad (2.4)$$

$$\mathbf{Z}_3 = \text{col}(0, -i/\sqrt{2}, 1, -i/\sqrt{2}, 1), \quad (2.5)$$

$$\lambda_2 = i[2a^2 + (\Delta b)^2]^{1/2}, \quad (2.6)$$

$$\lambda_3 = ia\sqrt{2}, \quad (2.7)$$

where $\text{col}(X_1, X_2, \dots)$ is a column vector of compounds X_1, X_2, \dots . The three functions η , ζ , and ξ depend on the slow time s and are yet undetermined. At the second in ϵ , we get a set of inhomogeneous differential equations for the variables $\psi_2, X_2, Y_2, \bar{X}_2$, and \bar{Y}_2 . Imposing these solutions to be bounded and periodic in T leads to the solvability condition which provides the equations

$$\begin{aligned} \eta_{s_1} = & 2a^2 D - (1 + a^2)(\Delta b)^2 \eta + a^2(2b_1 + \Delta b)\eta^2 \\ & - 4a^2(2b_1 + \Delta b)(\Delta b)^2 [3a^2 + (\Delta b)^2] r^2, \end{aligned} \quad (2.8)$$

$$r_{s_1} = -(1 + a^2)a^2 r + (2b_1 + \Delta b)[a^2(\Delta b)^2] \eta r, \quad (2.9)$$

$$\vartheta_{s_1} = 0, \quad (2.10)$$

$$\xi_{s_1} = -(1 + a^2)\xi/2, \quad (2.11)$$

where $s_1 = s/[2a^2 + (\Delta b)^2]$ and $\zeta = re^{i\vartheta}$. From Eq. (2.11) we observe that $\xi \rightarrow 0$ in the long-time limit. The remaining equations admit two steady-state solutions: (i)

$$r = 0, \quad \eta = \eta_{\pm}, \quad (2.12)$$

where η_{\pm} are the roots of $2a^2 D - (1 + a^2)(\Delta b)^2 \eta + a^2(2b_1 + \Delta b)\eta^2 = 0$ with the convention that $\eta_- > \eta_+$. This solution corresponds to steady-state solutions of Eqs. (1.10). The two values of η determine the two branches of the finite amplitude steady state. The condition that η be real leads to the restriction

$$D \leq D_L \equiv (1 + a^2)^2 (\Delta b)^4 / [8a^4(b_1 + b_2)]. \quad (2.13)$$

A linear stability analysis of the steady-state solution (2.12) gives the result that in the parameter domain defined by (2.13) the lower branch η_- is unstable, whereas the upper branch η_+ is stable if either $\Delta b < a$ or if $\Delta b > a$ and $D \leq D_H (< D_L)$. (ii)

$$\eta_P = (1 + a^2)a^2 / \{(2b_1 + \Delta b)[a^2 + (\Delta b)^2]\}, \quad r = r_P \neq 0, \quad (2.14)$$

where r_P is given by (2.8). In this case the steady-state solution (2.14) corresponds to a periodic solution of Eqs. (1.10). For the solution r_P to be real it is necessary that

$$D \geq D_H \equiv (1 + a^2)^2 \frac{[(\Delta b)^4 + a^2(\Delta b)^2 - a^4]}{2(2b_1 + \Delta b)[a^2 + (\Delta b)^2]^2}. \quad (2.15)$$

When this condition is verified, a linear stability analysis of (2.14) indicates that this solution is stable if $\Delta b > a$ and unstable when $\Delta b < a$. Thus for $\Delta b < a$ the unstable periodic solution emerges from the lower branch whereas for $\Delta b > a$ the stable periodic solution emerges from the upper stable branch. These two situations are displayed on Figs. 2 and 3 where we plot the maximum of E_2 [determined by a direct integration of Eqs. (1.10)] versus the control parameter θ . A point which is clearly shown on these figures is the fact that the stability property of the solutions near the limit point can change at a finite distance of the limit point.

When $\Delta b = a$ Eqs. (2.8) and (2.9) can be integrated exactly to give the undamped solutions:

$$\begin{aligned} \eta = & \eta_P - 4r_P E_0 \sin(s_2 + \psi_0) / [(r_P^2 + E_0^2)^{1/2} \\ & - E_0 \cos(s_2 + \psi_0)], \end{aligned} \quad (2.16)$$

$$r = r_P^2 / [(r_P^2 + E_0^2)^{1/2} - E_0 \cos(s_2 + \psi_0)] \quad (2.17)$$

with $s_2 = 8r_P a^2(2b_1 + a)s/3$. This corresponds to the solutions of a conservative system where E_0 and ψ_0 are

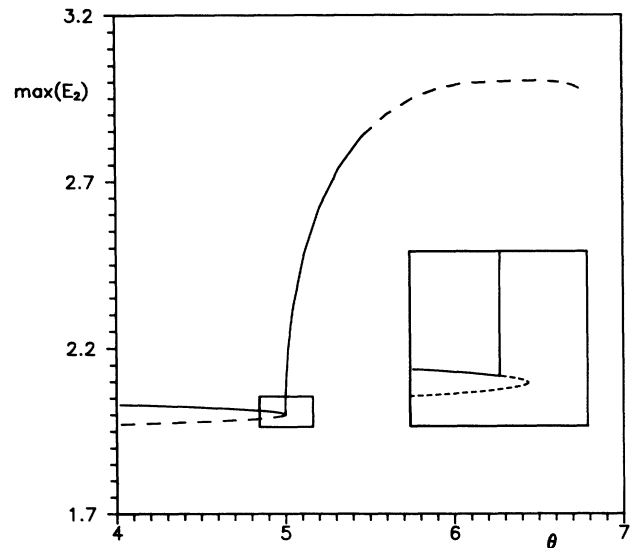


FIG. 2. Bifurcation diagram displaying the maximum of the field amplitude E_2 vs the control parameter θ with a supercritical Hopf bifurcation emerging near the limit point on the stable upper steady-state branch. In all figures, solid lines indicate stable solutions and dotted lines indicate unstable solutions. The parameters are $A_1 - 1 = A_2 - 1 = a^2 = 4$, $b_1 = 1$, $b_2 = 4$. For all figures we have taken $\epsilon = 0.01$. The condition $\Delta b > a$ is fulfilled.

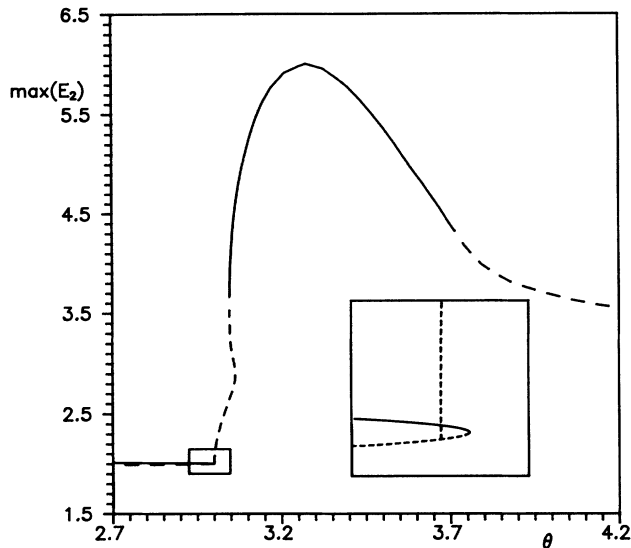


FIG. 3. Bifurcation diagram displaying the maximum of the field amplitude E_2 vs the control parameter θ with a subcritical Hopf bifurcation emerging near the limit point on the unstable lower steady-state branch. The parameters are $A_1 - 1 = A_2 - 1 = a^2 = 4$, $b_1 = 1$, $b_2 = 2$. The condition $\Delta b < a$ is fulfilled.

constants of integration representing the amplitude and phase of the periodic solutions, respectively. When the amplitudes α and β are periodic, the solution of Eqs. (1.10) is quasiperiodic. Unfortunately, the analysis of the third-order equations in ϵ (i.e., the study of ψ_3 , X_3 , Y_3 , \bar{X}_3 , and \bar{Y}_3) yields only the functional dependence of E_0 on ψ_0 . Thus the fourth-order equations at least are necessary to fully determine analytically the quasiperiodic solution. This has not been carried through.

III. IDENTICAL COUPLINGS BUT DIFFERENT PUMP PARAMETERS

A. Analytical results

In this section we analyze the vicinity of the limit point when the two coupling coefficients are equal but we allow the pump parameters to be different:

$$a_1 \neq a_2, \quad b_1 = b_2. \quad (3.1)$$

For convenience, we define the variables

$$d_{\pm} = a_2^2 \pm a_1^2, \quad d = bd_- / (a_1 a_2), \quad \Delta = [(d^2 - 2d_+)^2 - 16a_1^2 a_2^2]^{1/2}. \quad (3.2)$$

In this case the solution of the first-order equations Eqs. (1.10) is

$$\mathbf{V}(T, s) = \alpha(s) \mathbf{V}_1 + \beta_1(s) \mathbf{V}_2 \exp(i\Omega_1 T) + \beta_2(s) \mathbf{V}_3 \exp(i\Omega_2 T) + \text{c.c.}, \quad (3.3)$$

where

$$\mathbf{V} = \text{col}(\psi_1, X_1, Y_1, \bar{X}_1, \bar{Y}_1),$$

$$\mathbf{V}_1 = \text{col}(a_1 a_2, 0, b a_2^2, 0, b a_1^2), \quad (3.4)$$

$$\mathbf{V}_2 = \text{col}\{-d_-^2 + (d^2 + \Delta)^2/4, i\Omega_1 b a_2[-d_- + (d^2 + \Delta)/2], -2b a_1 a_2[-d_- + (d^2 + \Delta)/2], \\ i\Omega_1 b a_1[d_- + (d^2 + \Delta)/2], -2b a_1 a_2[d_- + (d^2 + \Delta)/2]\}, \quad (3.5)$$

$$\mathbf{V}_3 = \text{col}\{-d_-^2 + (d^2 - \Delta)^2/4, i\Omega_2 b a_2[-d_- + (d^2 - \Delta)/2], -2b a_1 a_2[-d_- + (d^2 - \Delta)/2], \\ i\Omega_2 b a_1[d_- + (d^2 - \Delta)/2], -2b a_1 a_2[d_- + (d^2 - \Delta)/2]\}, \quad (3.6)$$

$$\Omega_1^2 = d_+ + (d^2 + \Delta)/2, \quad (3.7)$$

$$\Omega_2^2 = d_+ + (d^2 - \Delta)/2. \quad (3.8)$$

Using the second-order expansion in ϵ of Eqs. (1.10) we get as in Sec. II a solvability condition which will be expressed as a set of differential equations for the three slowly varying amplitudes:

$$\alpha_s = (C_1 \alpha^2 + C_2 \alpha + B_1 |\beta_1|^2 + B_2 |\beta_2|^2 + D_1) / L_1, \quad (3.9)$$

$$\beta_{1s} = (F_1 + F_2 \alpha) \beta_1 / L_2, \quad (3.10)$$

$$\beta_{2s} = (G_1 + G_2 \alpha) \beta_2 / L_3. \quad (3.11)$$

The various parameters appearing in Eqs. (3.9)–(3.11) are defined in the Appendix.

Equations (3.9)–(3.11) have three different steady-state solutions: (i)

$$\beta_1 = \beta_2 = 0, \quad \alpha = \alpha_{\pm} = [-C_2 \pm (C_2^2 - 4D_1 C_1)^{1/2}] / 2C_1. \quad (3.12)$$

The condition for α_{\pm} to be real can be expressed as a condition on the detuning:

$$D \leq D_L \equiv C_2^2 / (8a_1^2 a_2^2 C_1). \quad (3.13)$$

(ii)

$$\beta_2 = 0, \quad \alpha = -F_1 / F_2, \\ |\beta_1|^2 = -(C_1 F_1^2 - C_2 F_1 F_2 + D_1 F_2^2) / (B_1 F_2^2). \quad (3.14a)$$

This solution exists if and only if (iff)

$$B_1 > 0, D < D_{H1} \text{ or } B_1 < 0, D > D_{H1}, \quad (3.14b)$$

with

$$D_{H1} = F_1(C_2 F_2 - C_1 F_1) / (2a_1^2 a_2^2 F_2^2).$$

(iii)

$$\begin{aligned} \beta_1 &= 0, \alpha = -G_1/G_2, \\ |\beta_2|^2 &= -(C_1 G_1^2 - C_2 G_1 G_2 + D_1 G_2^2) / (B_2 G_2^2). \end{aligned} \quad (3.15a)$$

This solution exists iff

$$B_2 > 0, D < D_{H2} \text{ or } B_2 < 0, D > D_{H2}, \quad (3.15b)$$

with

$$D_{H2} = G_1(C_2 G_2 - C_1 G_1) / (2a_1^2 a_2^2 G_2^2).$$

The linear stability of these solutions is easily determined. For the solutions (i) we find that α_+ is always unstable whereas α_- is stable when the two following conditions are verified:

$$\begin{aligned} 2C_1 F_1 - C_2 F_2 - F_2(C_2^2 - 4D_1 C_1)^{1/2} &< 0, \\ 2C_1 G_1 - C_2 G_2 - G_2(C_2^2 - 4D_1 C_1)^{1/2} &< 0. \end{aligned} \quad (3.16)$$

The solution (ii) is stable either if

$$F_2 > 0, 2C_1 F_1 - C_2 F_2 > 0, B_1 < 0, G_1 F_2 - G_2 F_1 < 0, \quad (3.17a)$$

or if

$$F_2 < 0, 2C_1 F_1 - C_2 F_2 < 0, B_1 > 0, G_1 F_2 - G_2 F_1 > 0. \quad (3.17b)$$

Similarly, the solution (iii) is stable either if

$$G_2 > 0, 2C_1 G_1 - C_2 G_2 > 0, B_2 < 0, G_1 F_2 - G_2 F_1 < 0, \quad (3.18a)$$

or if

$$G_2 < 0, 2C_1 G_1 - C_2 G_2 < 0, B_2 > 0, G_1 F_2 - G_2 F_1 > 0. \quad (3.18b)$$

Although we did not pursue the calculation further on, it is worth noticing that when $2C_1 F_1 = C_2 F_2$ the function β_1 undergoes a Hopf bifurcation corresponding to quasi-periodic solutions of Eqs. (1.10). In a similar way, when $2C_1 G_1 = C_2 G_2$ the function β_2 undergoes a Hopf bifurcation corresponding to a quasiperiodic solution of Eqs. (1.10) but with another pair of frequencies.

B. Numerical results

In this section we determine some properties of the complete set of nonlinear equations Eqs. (1.1) which we write with the normalized variables (1.6)–(1.9) as

$$\Delta\mu' = \theta - [(b_1 E_2 / E_1) + (b_2 E_1 / E_2)] \sin(\Delta\mu), \quad (3.19a)$$

$$E_1' = E_1 W_1 + b_1 E_2 \cos(\Delta\mu), \quad (3.19b)$$

$$W_1' = a_1^2 - E_1^2 - \epsilon W_1(1 + E_1^2), \quad (3.19c)$$

$$E_2' = E_2 W_2 + b_2 E_1 \cos(\Delta\mu), \quad (3.19d)$$

$$W_2' = a_2^2 - E_2^2 - \epsilon W_2(1 + E_2^2). \quad (3.19e)$$

Unless otherwise explicitly stated, we took $\gamma = 10^{-4}$ (i.e., $\epsilon = 10^{-2}$) to adhere to experimental values. All parameters are chosen in such a way that they verify the operating conditions (1.4). Furthermore, within this range we selected parameter values that best display the bifurcation structure of the problem. In Fig. 4 we have drawn three boundaries in the (a_1^2, a_2^2) plane. The boundaries B_I and B_{II} are derived respectively from the equations

$$b^2 \geq 2a_1^2 a_2^2 / (a_1 - a_2)^2, \quad (3.20)$$

$$b^2 \leq 2a_1^2 a_2^2 / (a_1 + a_2)^2, \quad (3.21)$$

which are necessary to ensure that the function Δ defined in (3.2) remains real. These two conditions are sufficient and necessary for the solution $\mathbf{V}(T, s)$ defined by (3.3) to be periodic. In (3.20) and (3.21) the equality sign defines the boundaries B_I and B_{II} .

In the domain lying between the axes and the B_I boundary, a numerical study indicates that the upper branch α_- of the steady-state solution (3.12) is stable in the vicinity of the limit point as long as $D < D_{H1}$ ($< D_L$). This branch of steady-state solutions loses its stability via a Hopf bifurcation when $D = D_{H1}$ and the periodic solution (3.14a) is stable with frequency Ω_1 above but near to the Hopf bifurcation.

Between the two boundaries B_I and B_{II} our analytical treatment is not valid since the Hopf bifurcation is not near the limit point. Thus there are no analytical results with which to compare the numerical integrations of Eqs.

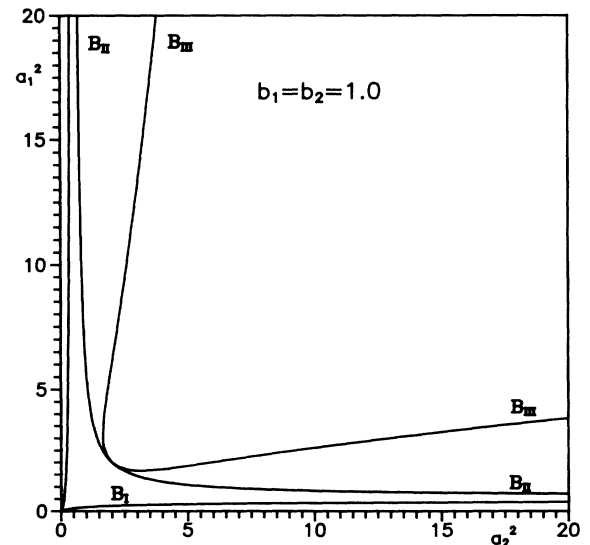


FIG. 4. Stability boundaries for the steady, periodic, and quasiperiodic solutions.

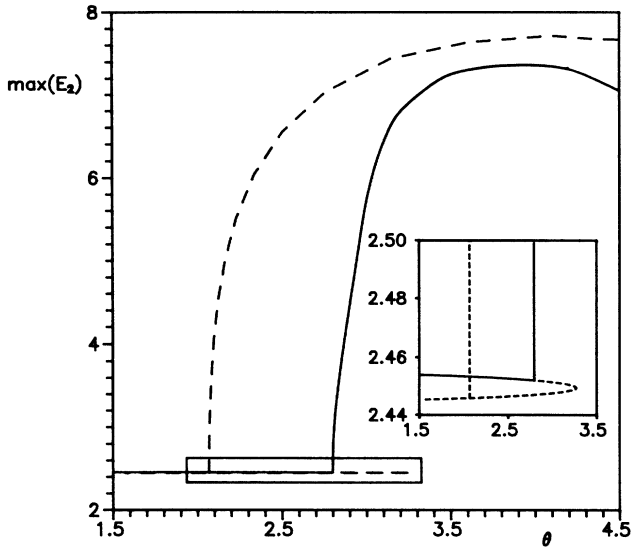


FIG. 5. Bifurcation diagram displaying two Hopf bifurcations near the limit point, each emerging from a different steady-state branch. Parameters are $a_1^2=0.7$, $a_2^2=6$, $b_1=b_2=1$. The representative point in the parameter space of Fig. 4 lies between the boundaries B_I and B_{II} .

(3.19) which show domains of stable and unstable periodic solutions. An example of the bifurcation diagram in this domain is displayed on Fig. 5.

Near but above the boundary B_{II} the steady-state solu-

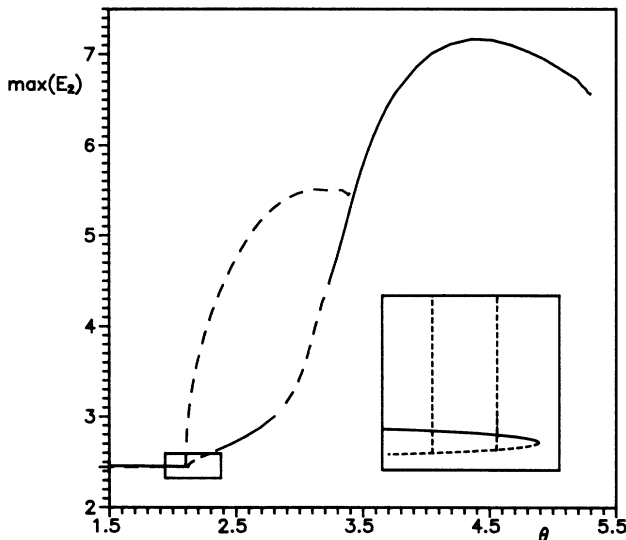


FIG. 6. Bifurcation diagram displaying two Hopf bifurcation near the limit point, both emerging from the unstable steady-state branch. Parameters are $a_1^2=3$, $a_2^2=6$, $b_1=b_2=1$. The representative point in the parameter space of Fig. 4 lies well above the boundary B_{III} . The branch of periodic solutions which starts nearest from the limit point is first unstable, then undergoes three changes of stability within the domain displayed on the figure.

tion α_- is stable if either $V_2 > 0$ and $D < D_{H2}$ ($< D_L$) or $V_2 < 0$ and $D < D_L$. However, when $V_2 > 0$ and $D > D_{H2}$, a Hopf bifurcation occurs and the solution (3.15a) becomes stable with frequency Ω_2 . When the stable periodic regime has been established, a further bifurcation occurs when $V_2=0$. At this point a quasiperiodic solution emerges. The boundary $V_2=0$ corresponds to the

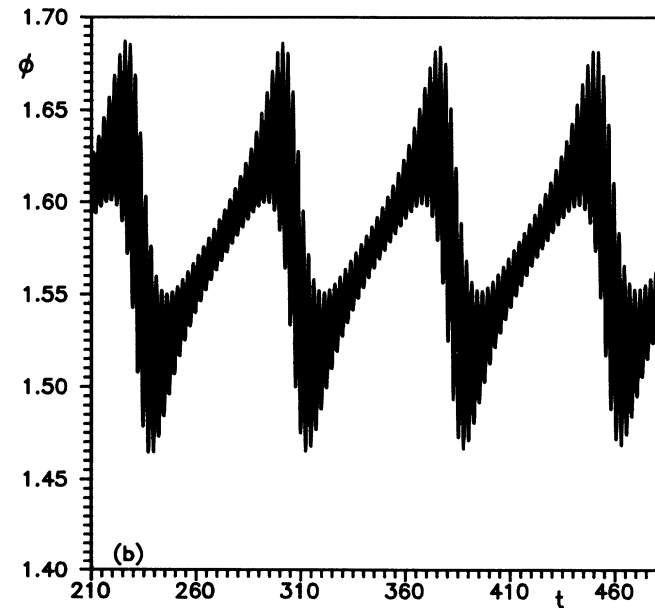
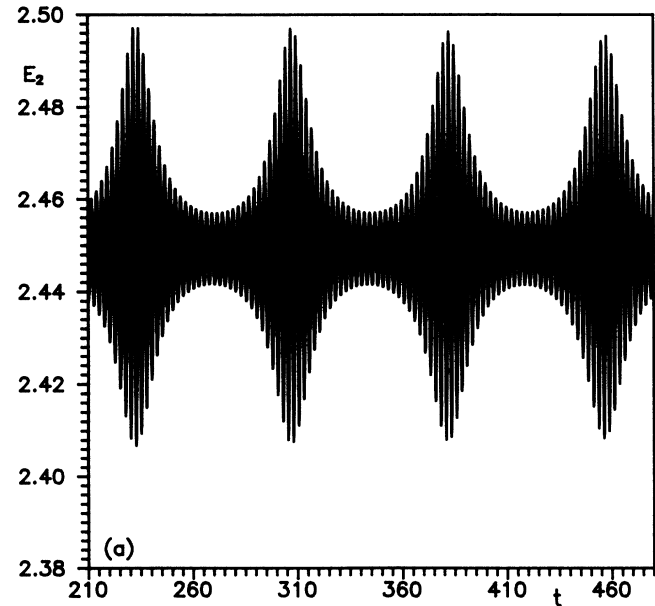


FIG. 7. The solution of Eqs. (1) for the field amplitude and phase in the stable quasiperiodic regime. Parameters are $a_1^2=2$, $a_2^2=6$, $b_1=b_2=1$, $D=2.313$. The representative point in the parameter plane in Fig. 4 is slightly above the B_{III} boundary.

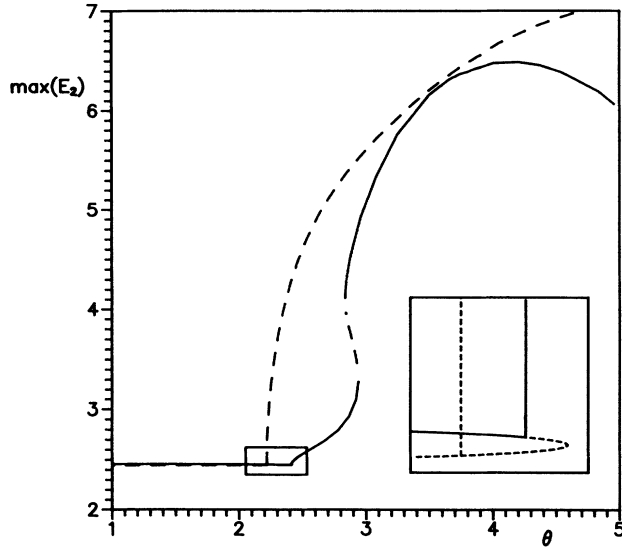


FIG. 8. Bifurcation diagram displaying two Hopf bifurcations near the limit point, each emerging from a different steady-state branch. Parameters are $a_1^2=1.7$, $a_2^2=6$, $b_1=b_2=1$. The representative point in the parameter space of Fig. 4 lies between the boundaries B_{II} and B_{III} . Note the bistability between the small and the large amplitude solutions.

line B_{III} on Fig. 4. To exemplify the behavior of the solutions in the various domains defined by the three boundaries, we have made a vertical scan in the parameter plane represented in Fig. 4 along the line $A_2 - 1 = a_2^2 = 6$. In Fig. 6 we give the bifurcation diagram for a point

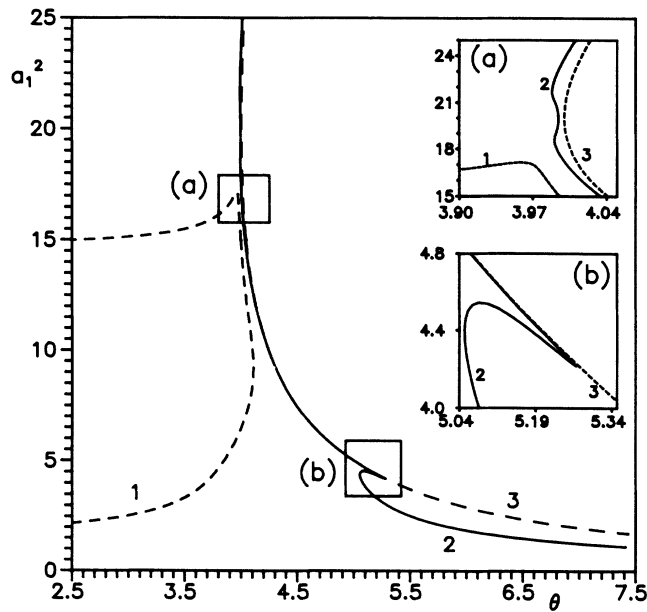
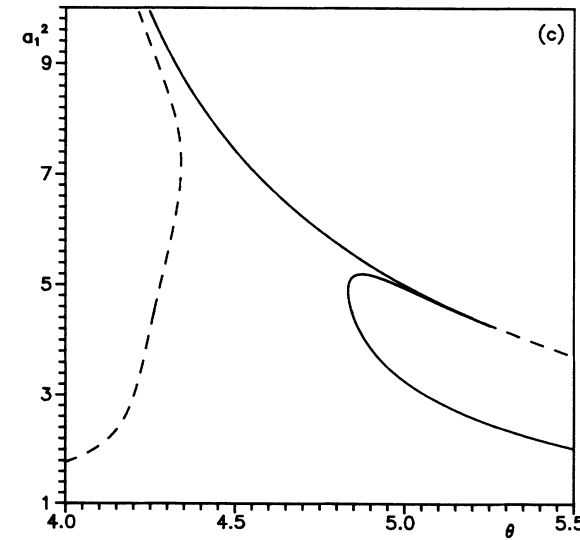
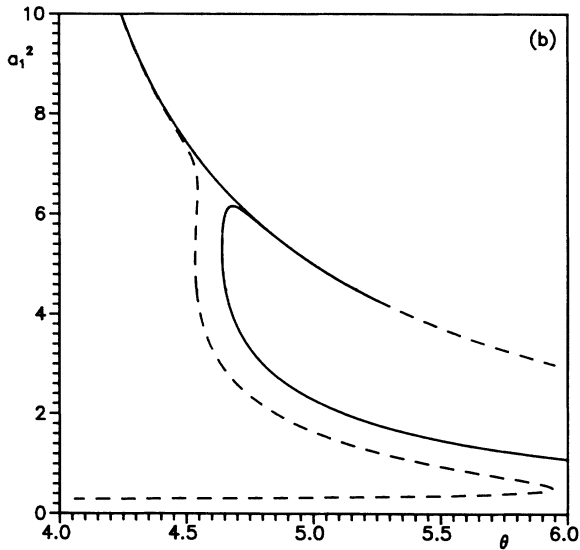
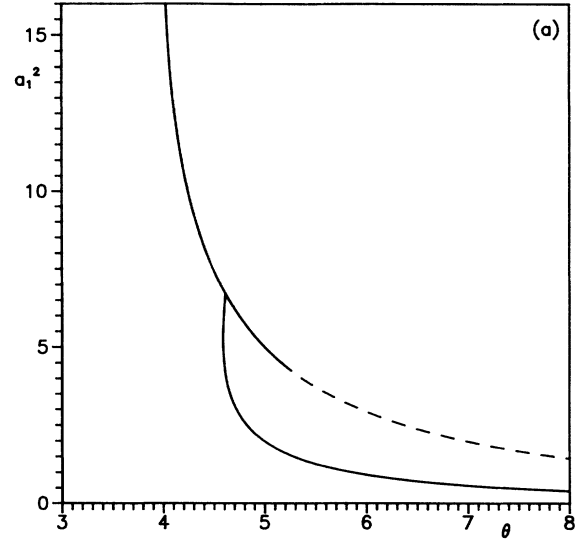


FIG. 9. Stability boundaries in the (a_1^2, θ) parameter plane. The boundary 3 is the locus of limit points whereas the boundaries 1 and 2 are loci of Hopf bifurcations. Parameters are $a_2^2=20$ and $b=2$.

FIG. 10. The evolution of the window (b) of Fig. 9 with $\epsilon=0$ in (a), $\epsilon=0.001$ in (b) and $\epsilon=0.005$ in (c). The other parameters are $a_2^2=20$ and $b=2$.

which lies well beyond the B_{III} boundary. It is seen that the two Hopf bifurcations are subcritical, leading to unstable limit cycles. One of the periodic solutions remains unstable, whereas the other solution has two domains of stable periodic solutions at an $O(1)$ distance from the bifurcation point. On Figs. 7 we display the field phase and amplitude in the quasiperiodic regime. On Fig. 8 the bifurcation diagram corresponds to a point which lies between the boundaries B_{II} and B_{III} . The periodic solution emerging from the unstable branch is unstable and remains so for the parameter values considered. On the contrary, a stable periodic solution emerges from the upper branch near to the limit point and enters a bistable loop involving a small and a large intensity periodic solutions.

Finally in Fig. 9 we display the stability boundaries for the solutions of Eqs. (3.19) in the (a_1^2, θ) parameter plane. The boundaries 1 and 2 are loci of Hopf bifurcation whereas the boundary labeled 3 is the locus of the limit point. Our analytical results hold only when the boundaries 2 and 3 are close to each other. This occurs in a domain clearly shown on the figure with a distance between the two boundaries being of order ϵ^2 . A similar closeness of the two boundaries occurs for large θ or small a_1^2 . The domain between the boundaries B_I and B_{II} on Fig. 4. corresponds to the domain where the boundaries 2 and 3 are not close to each other.

It is useful to consider how the diagram shown on Fig. 9 depends on the smallness parameter ϵ . Figures 10(a)–10(c) indicate how the domain around the window labeled b on Fig. 9 evolves as ϵ increases from zero to 0.01. We see that in the limit $\epsilon \rightarrow 0$ four loci of Hopf bifurcations tend to coincide pairwise and are indeed degenerate when ϵ exactly vanishes. This is shown in an alternative way on the remaining two figures. On Fig. 11 we set $\epsilon = 0$; the nearly horizontal line is the steady state

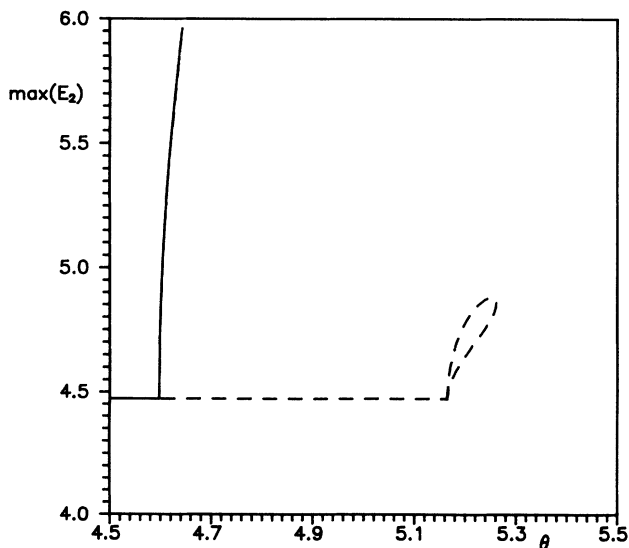


FIG. 11. Degenerate bifurcation diagram for $\epsilon=0$, $a_1^2=4.5$, $a_2^2=20$ and $b=2$.

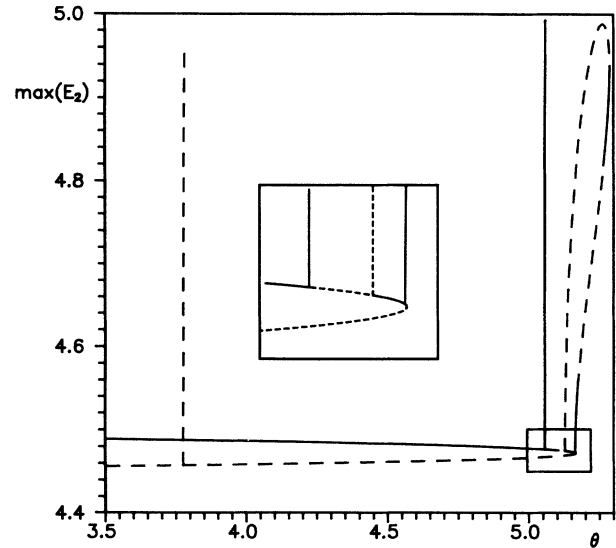


FIG. 12. Same as Fig. 11 but with $\epsilon=0.01$.

which is stable for small values of θ . Because $\epsilon=0$ there is also a collapse of the two branches of steady state into a unique state. It becomes unstable via a Hopf bifurcation. What cannot be shown on the figure is that two Hopf bifurcations occur exactly at the same point, out of which one periodic solution is stable and the other is unstable. The same phenomenon appears for larger θ where two Hopf bifurcations coincide with the limit point. Here the situation is easier to understand since we have been able to completely follow the unstable periodic solution. Finally on Fig. 12 the same situation is considered but with $\epsilon=0.01$. It is easy to see how $\epsilon \neq 0$ lifts the degeneracies. First, there are now two steady states and in both cases the two degenerate Hopf bifurcations are split. The pair of Hopf which occurred at low θ are separated, being each on a different branch. They retain their stability properties near the bifurcation point. The pair of Hopf at the limit point move both on the upper branch of steady solution. Of this pair the first bifurcation is subcritical and restores the stability of the steady state. The second Hopf is supercritical and leads to stable periodic solutions and the steady state is again unstable until the limit point. Note that there is a further change of stability far from the Hopf: there also are two critical points which determine a domain of stable periodic solutions which merge in the limit $\epsilon \rightarrow 0$. In this case the stable periodic solution which emerges from the steady state becomes unstable to yield quasiperiodic solutions. They correspond to the solutions of Eqs. (3.10) and (3.11) with $\beta_1 \neq 0$ and $\beta_2 \neq 0$.

ACKNOWLEDGMENTS

Partial support from the Fonds National de la Recherche Scientifique and the Interuniversity Attraction Pole of the Belgian government is gratefully acknowledged.

APPENDIX

The coefficients of Eqs. (3.9)–(3.11) are

$$\begin{aligned}
 B_1 &= 2ba_1a_2d^2[-d_+^2 + (\Delta + d^2)/2] \\
 &\quad \times [2d^2d_+^2 + 4a_1^2a_2^2d_+ - (d^2 + \Delta)(4a_1^2a_2^2 + d^2d_+)] , \\
 B_2 &= 2ba_1a_2d^2[-d_+^2 + (d^2 - \Delta)/2] \\
 &\quad \times [2d^2d_+^2 + 4a_1^2a_2^2d_+ - (d^2 - \Delta)(4a_1^2a_2^2 + d^2d_+)] , \\
 C_1 &= a_1^3a_2^3bd_+ , \\
 C_2 &= -a_1a_2d^2(d_+ + a_1^2a_2^2) , \\
 D_1 &= 2a_1^2a_2^2D , \\
 F_1 &= 2a_1^3a_2^3d^2[(d^2 + \Delta)^2/4 + 2(d^2 + \Delta) \\
 &\quad + (d^2 + \Delta)d_+ + d_-^2] ,
 \end{aligned}$$

$$\begin{aligned}
 F_2 &= a_1a_2bd^2[-d_+ + (d^2 + \Delta)/2] \\
 &\quad \times [(d^2 + \Delta)(d_+d^2 + 2a_1^2a_2^2) - 2d^2d_+^2] , \\
 G_1 &= 2a_1^3a_2^3d^2[(d^2 - \Delta)^2/4 + 2(d^2 - \Delta) \\
 &\quad + (d^2 - \Delta)d_+ + d_-^2] , \\
 G_2 &= a_1a_2bd^2[-d_+ + (d^2 - \Delta)/2] \\
 &\quad \times [(d^2 - \Delta)(d_+d^2 + 2a_1^2a_2^2) - 2d^2d_+^2] , \\
 L_1 &= a_1a_2(2a_1^2a_2^2 + d^2d_+) , \\
 L_2 &= a_1a_2d^2[\Delta^2d^2 - \Delta(2d^2d_+ - d^4 + 8a_1^2a_2^2)] , \\
 L_3 &= a_1a_2d^2[\Delta^2d^2 + \Delta(2d^2d_+ - d^4 + 8a_1^2a_2^2)] .
 \end{aligned}$$

*On leave of absence from the Beijing Normal University.

¹P. Mandel, Li R. D., and T. Erneux, *Phys. Rev. A* **39**, 2502 (1989).

²N. M. Lawandy and K. Lee, *Opt. Commun.* **61**, 137 (1987).

³N. M. Lawandy, D. V. Plant, and K. Lee, *Phys. Rev. A* **34**, 1247 (1987).

⁴T. Erneux, S. M. Baer, and P. Mandel, *Phys. Rev. A* **35**, 1165 (1987).

⁵G. L. Oppo and A. Politi, *Z. Phys. B* **59**, 111 (1985).

⁶S. S. Wang and H. G. Winful, *Appl. Phys. Lett.* **52**, 23 (1988).

⁷S. E. Falvey and W. W. Chow, *J. Opt. Soc. Am. B* **6**, 1894 (1989).

⁸G. L. Oppo, A. Politi, G. L. Lippi, and F. T. Arecchi, *Phys. Rev. A* **34**, 4000 (1986).

⁹Koncay and H. and Pei Yu, *Can. Math. Soc. Conf. Proc.* **8**, 465 (1987).

¹⁰*J. Opt. Am. B* **2**, 5 (1985); *Coherence and Quantum Optics*, edited by L. Mandel and E. Wolf (Plenum, New York, 1984).